

# Features of holographic dark energy under the combined cosmological constraints

Yin-Zhe Ma,<sup>1,2,\*</sup> Yan Gong,<sup>3,†</sup> and Xuelei Chen<sup>3,1,‡</sup>

<sup>1</sup>*Kavli Institute for Theoretical Physics China,*

*Institute of Theoretical Physics, Chinese Academy of Sciences,*

*P.O.Box 2735, Beijing 100080, China*

<sup>2</sup>*Institute of Astronomy, University of Cambridge,*

*Madingley Road, Cambridge, CB3 0HA, U.K.*

<sup>3</sup>*National Astronomical Observatories,*

*Chinese Academy of Sciences, Beijing 100012, China*

We investigate the observational signatures of the holographic dark energy models in this paper, including both the original model and a model with an interaction term between the dark energy and dark matter. We first delineate the dynamical behavior of such models, especially whether they would have “Big Rip” for different parameters, then we use several recent observations, including 182 high-quality type Ia supernovae data observed with the Hubble Space Telescope, the SNLS and ESSENCE surveys, 42 latest Chandra X-ray cluster gas mass fraction, 27 high-redshift gamma-ray burst samples, the baryon acoustic oscillation measurement from the Sloan Digital Sky Survey, and the CMB shift parameter from WMAP three years result to give more reliable and tighter constraints on the holographic dark energy models. The results of our constraints for the holographic dark energy model without interaction is  $c = 0.748^{+0.108}_{-0.009}$ ,  $\Omega_{m0} = 0.276^{+0.017}_{-0.016}$ , and for model with interaction ( $c = 0.692^{+0.135}_{-0.107}$ ,  $\Omega_{m0} = 0.281^{+0.017}_{-0.017}$ ,  $\alpha = -0.006^{+0.021}_{-0.024}$ , where  $\alpha$  is an interacting parameter). As these models have more parameters than the  $\Lambda$ CDM model, we use the Bayesian evidence as a model selection criterion to make comparison. We found that the holographic dark energy models are mildly favored by the observations compared with the  $\Lambda$ CDM model.

---

\*Electronic address: yzm20@cam.ac.uk

## I. INTRODUCTION

It has been realized that our Universe is experiencing an accelerated expansion, as shown by several astronomical observations [1]. The acceleration of the Universe strongly indicates the existence of a mysterious exotic matter, namely the dark energy, which has large enough negative pressure and makes up the largest portion of the total matter in the current Universe. The combined analysis of observational data suggests that the Universe is spatially flat, and consists of approximately 3/4 dark energy, 1/4 dust matter (cold dark matter plus baryons), and negligible amount of radiation [1, 2, 3]. The simplest candidate of dark energy is the cosmological constant  $\Lambda$  (vacuum energy) which has the equation of state  $w = -1$ . The cosmological constant-cold dark matter model ( $\Lambda$ CDM) works very well, and is in agreement with a large number of recent observations. However, there are two problems in this scenario — the *fine-tuning* problem and the *cosmic coincidence* problem [4]. The fine-tuning problem asks why the vacuum energy density today is so small ( $10^{-47}\text{GeV}^4$ ) compared with the theoretical value ( $10^{74}\text{GeV}^4$ ) from the quantum gravity. The cosmic coincidence problem is that since the evolution of the energy densities of dark matter and dark energy are so different during the expansion of the Universe, why are they nearly equal to each other today?

The dark energy may be a problem which has to be solved in the context of quantum gravity [5]. In the classical gravity theory, the dark energy density (cosmological constant) can be an arbitrary value. However, a complete theory of quantum gravity should be capable of determining the properties of dark energy such as the energy density and the equation of state [5]. The holographic dark energy model is an attempt to apply the holographic principle of quantum gravity theory to the dark energy problem [6, 7, 8, 9].

It is well known that the holographic principle is an important result from the explorations of the quantum gravity theory and string theory [10], enlightened by investigations on the properties of black holes. For an effective field theory in a box of size  $L$  with UV cut-off  $\Lambda_c$ , the entropy  $S$  scales extensively as  $S \sim L^3 \Lambda_c^3$ . However, considering the peculiar thermodynamics of black hole [11], the maximum entropy in a box of volume  $L^3$  may

---

<sup>†</sup>Electronic address: gongyan@bao.ac.cn

<sup>‡</sup>Electronic address: xuelei@cosmology.bao.ac.cn

behave nonextensively, growing only as the surface area of the box, i.e.  $S \leq S_{\text{BH}} \equiv \pi M_{\text{pl}}^2 L^2$  (Bekenstein entropy bound). This nonextensive scaling suggests that quantum field theory breaks down in large volume. To reconcile this breakdown with the success of local quantum field theory, Cohen et al. [6] proposed a more restrictive energy bound. They pointed out that in quantum field theory a short distance (UV) cut-off is related to a long distance (IR) cut-off due to the limit set by forming a black hole. In other words, if the quantum zero-point energy density  $\rho_\Lambda$  is relevant to a UV cut-off, the total energy of the whole system with size  $L$  should not exceed the mass of a black hole of the same size, thus we have  $L^3 \rho_\Lambda \leq L M_{\text{pl}}^2$ . When we take the whole Universe into account, the vacuum energy related to this holographic principle [10] is viewed as dark energy, usually dubbed holographic dark energy. The largest IR cut-off  $L$  is chosen by saturating the inequality so that we get the holographic dark energy density

$$\rho_{\text{de}} = 3c^2 M_{\text{pl}}^2 L^{-2} , \quad (1)$$

where  $c$  is a numerical constant, and  $M_{\text{pl}} \equiv 1/\sqrt{8\pi G}$  is the reduced Planck mass. If we take  $L$  as the size of the current Universe, for instance the Hubble scale  $H^{-1}$ , then the dark energy density will be close to the observational result. However, Hsu [8] pointed out that this yields a wrong equation of state for dark energy. Li [9] subsequently proposed that the IR cut-off  $L$  should be taken as the size of the future event horizon

$$R_{\text{eh}}(a) = a \int_t^\infty \frac{dt'}{a(t')} = a \int_a^\infty \frac{da'}{H a'^2} . \quad (2)$$

Then this problem can be solved, and the holographic model can thus be constructed successfully. For extensive studies of this model (HDE), see Ref. [12, 13, 14, 15, 16, 17, 18, 19, 20, 21, 22, 23]. The holographic dark energy may also have interaction with matter, this is the so called interacting dark energy model (IHDE) [17, 18]. Both the HDE and IHDE model can be tested by cosmological observations, such as the type Ia supernovae [24], CMB [25, 26, 27], X-ray gas mass fraction in the clusters [28], differential ages of passively evolving galaxies [29] and combinations of SN Ia, CMB and LSS data [30, 31, 32, 33]. Currently, the tightest constraint on the HDE model is given by [32], namely  $c = 0.85^{+0.18}_{-0.02}$  and  $\Omega_{m0} = 0.27^{+0.04}_{-0.03}$ , but  $c > 1$  is still allowed under this constraint. In addition, by using the  $\chi^2$  statistic as a model comparison technique, Ref.[32] suggests that HDE model is equally favored by the current observational data compared with the  $\Lambda$ CDM model.

In this paper we consider the dynamical behavior of the holographic dark energy models, particularly what is the condition for the Universe to end in the so called “Big Rip” [34]. we then use several new data sets to constraint the holographic dark energy models. These includes a sample of 182 high quality SN Ia data (Despite coincidence in number, this is not exactly the same data set used by Gold06 [35]), a sample of 42 latest X-rays gas mass fraction ( $f_{\text{gas}}$ ) data [38], a sample of 27 gamma-ray burst (GRB) data[39] generated from one of the tightest correlations—the  $E_{\text{peak}} - E_{\gamma}$  correlation [40], the baryon acoustic oscillation measurement from the Sloan Digital Sky Survey[41], and the CMB shift parameter from WMAP 3 years result. With these more diverse set of observations, we can obtain constraints which are not only tighter, but also more reliable.

We compare the observational fit of the HDE and IHDE models with the  $\Lambda$ CDM model. In previous works, the  $\chi^2$  statistic has been used for comparison. However, as the holographic dark energy models (with or without interaction) have more parameters than the  $\Lambda$ CDM, the  $\chi^2$  may not be a suitable criterion for making comparison. Here we use the Bayesian Evidence (BE) as the information criterion to assess the strength of the holographic models.

The paper is organized as follows: In §2, we review our models of holographic dark energy, and derive the evolution equations. We also discuss qualitatively the behavior of the HDE and IHDE models, particularly the impact of the interacting term on the fate of the Universe. In §3, we present our method of analysis and the data used (§3A), then briefly discuss the Markov Chain Monte Carlo (MCMC) techniques (§3B) and the model selection criteria (§3C). In §4, we show the results of our constraints, and using the Bayesian evidence we make comparisons between the holographic dark energy models (including the HDE and IHDE) and the  $\Lambda$ CDM model. We summarize our result and conclude in §5.

## II. THE MODELS

For a spatially flat (the flat geometry is assumed throughout this paper) Friedmann-Robertson-Walker (FRW) Universe filled with matter component  $\rho_{\text{m}}$  and holographic dark energy  $\rho_{\text{de}}$ , the Friedmann equation reads

$$3M_{\text{pl}}^2 H^2 = \rho_{\text{m}} + \rho_{\text{de}} . \quad (3)$$

where  $\rho_{\text{de}} = 3c^2 M_{\text{pl}}^2 L^{-2}$ ,  $L$  is the future event horizon, i.e.  $L(t) = R_{\text{eh}}(a)$ .

When we consider the interaction term between the two dark components, the conservation equations can be written as

$$\dot{\rho}_m + 3H\rho_m = Q, \quad (4)$$

$$\dot{\rho}_{de} + 3H(1 + w_{de})\rho_{de} = -Q, \quad (5)$$

where  $w_{de}$  is the equation of state of holographic dark energy. The form of the interaction  $Q$  is not unique. Here, we consider an interaction term of the following form (similar to but slightly different from those given in [17]):

$$Q = 3\alpha H\rho_{de}, \quad (6)$$

This form of interaction has been discussed in some literatures on inflation and reheating. For example, in the warm inflationary model [42], in which the scalar field's energy is transferred to the matter due to scalar field oscillations, there is an interaction term which is throughout the inflationary regime (not just after slow-roll), so that the energy of the scalar field is transferred to the matter content continuously and the matter content is not driven to zero [43]. Also, in string theory, a similar interaction term arises in the Einstein frame which depends on the dark energy density. Moreover, a term of the form (6) could be motivated by analogy with dissipation, for instance, a fluid with bulk viscosity may give rise to a term of this form in the conservation equation [43, 44]. We note, however, that interactions of other form is also possible and has been discussed in the literature [45, 46, 47]

Using the definition of holographic dark energy (1) and the relationship  $\rho_{de} = 3H^2 M_{pl}^2 \Omega_{de}$  (in which  $\Omega_{de}$  is the fractional dark energy density), taking the derivative with respect to  $x = \ln a$ , we obtain

$$\rho'_{de} \equiv \frac{d\rho_{de}}{dx} = -6M_{pl}^2 H^2 \Omega_{de} \left(1 - \frac{\sqrt{\Omega_{de}}}{c}\right). \quad (7)$$

Considering the derivative relationship between  $t$  and  $z$ :  $\frac{d}{dt} = H \frac{d}{dx} = -H(1+z) \frac{d}{dz}$  and Eq. (5) and (6), we have the following equation

$$\rho'_{de} + 3(1 + w_{de})\rho_{de} = -3\alpha\rho_{de}. \quad (8)$$

After taking derivative about  $\rho_{de} = 3H^2 M_{pl}^2 \Omega_{de}$  and substitute Eq.(7) into it, we obtain

$$\frac{H'}{H} = -\frac{\Omega'_{de}}{2\Omega_{de}} + \frac{\sqrt{\Omega_{de}}}{c} - 1. \quad (9)$$

On the other hand, using the Friedmann equation  $\dot{H} = -\frac{1}{2M_{\text{pl}}^2}(\rho + p)$  ( $\rho$  and  $p$  are the total energy density and pressure), and substitute  $\dot{H} = H'H$  and  $w_{\text{de}}$  from Eq. (8) into it, we could get

$$\frac{H'}{H} = \frac{1}{2}\Omega_{\text{de}} - \frac{3}{2} + \frac{1}{c}\Omega_{\text{de}}^{\frac{3}{2}} + \frac{3}{2}\alpha\Omega_{\text{de}}. \quad (10)$$

Combining Eq. (9) and (10), we find the differential equation for  $\Omega_{\text{de}}$

$$\frac{d\Omega_{\text{de}}(z)}{dx} = \Omega_{\text{de}}[(1 - \Omega_{\text{de}})(1 + \frac{2}{c}\sqrt{\Omega_{\text{de}}}) - 3\alpha\Omega_{\text{de}}], \quad (11)$$

i.e.

$$\frac{d\Omega_{\text{de}}(z)}{dz} + \frac{\Omega_{\text{de}}}{1+z}[(1 - \Omega_{\text{de}})(1 + \frac{2}{c}\sqrt{\Omega_{\text{de}}}) - 3\alpha\Omega_{\text{de}}] = 0. \quad (12)$$

Consequently, the differential equation for Hubble parameter  $H(z)$  could be written as

$$\frac{dH}{dz} = -\frac{H(z)}{1+z}[\frac{1}{2}\Omega_{\text{de}}(1 + 3\alpha + \frac{2}{c}\sqrt{\Omega_{\text{de}}}) - \frac{3}{2}]. \quad (13)$$

Eq.(12) and (13) can be solved numerically to obtain the expansion rate  $H(z)$ .

We now study the behavior of the holographic dark energy models. The evolution of dark energy can be understood by inspecting its effective equation of state, for which we have

$$\rho'_{\text{de}} + 3(1 + w_{\text{eff}})\rho_{\text{de}} \equiv 0. \quad (14)$$

Using Eqs.(7) and (8) we obtain

$$w_{\text{eff}}(z) = w_{\text{de}} + \alpha = -\frac{1}{3} - \frac{2}{3}\frac{\sqrt{\Omega_{\text{de}}}}{c}. \quad (15)$$

It is interesting to note here that  $\alpha$  (i.e. the interaction rate of dark energy and dark matter) does NOT show up explicitly in this equation, but only implicitly affects the result through its effect on  $\Omega_{\text{de}}$ , so this equation applies to both HDE and IHDE models. For the flat Universe with dark energy, the dark energy would eventually dominate the density,  $\Omega_{\text{de}} \rightarrow 1$ , hence the effective equation of state of the holographic dark energy evolves dynamically, and

$$w_{\text{eff}} \rightarrow -\frac{1}{3} - \frac{2}{3c}. \quad (16)$$

It is obvious from Eqs. (15)-(16) that for the HDE model, the equation of state depends on the parameter  $c$ . For  $c > 1$ , the equation of state  $w > -1$ , and the holographic dark energy behaves as quintessence. For  $c < 1$ ,  $w < -1$  could be realized. For such models, the Universe would end in a Big Rip.

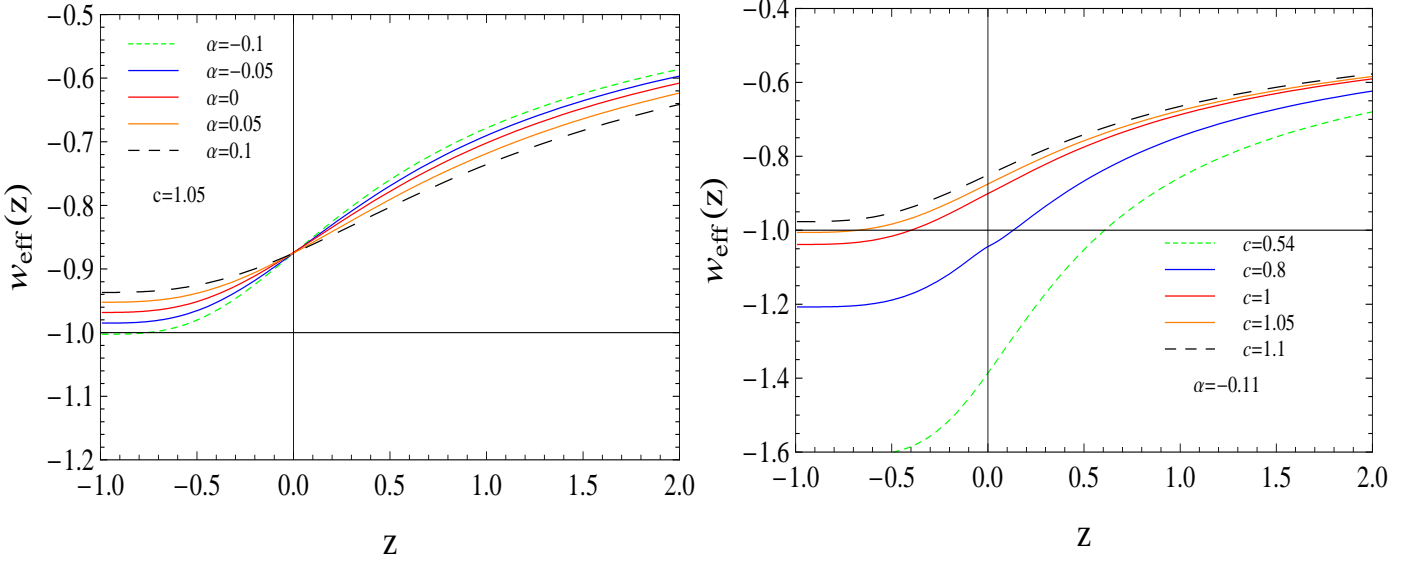


FIG. 1: Equation of state for the selected values of  $(c, \alpha)$  or the illustration purpose. Here we set  $\Omega_{m0} = 0.27$ .

For IHDE models, we illustrate the behavior of the model by choosing some representative values of  $\alpha$  and  $c$ , and plot the evolution of equation of state  $w(z)$  in Fig. 1. On the left of Fig. 1, we show the evolution of equation of state  $w$  as a function of  $z$  for fixed value of  $c$  ( $c = 1.05$ ) and different values of  $\alpha$ . Initially, all models have  $-1 < w_{\text{eff}} < 0$ . If  $\alpha = 0$ , the model is reduced to the case of HDE, for which the equation of state  $w \rightarrow -1$  (cosmological constant) as  $z \rightarrow -1$  ( $a \rightarrow \infty$ ). For  $\alpha > 0$ , energy is transferred from dark energy to dark matter, making the effective equation of state of the dark energy greater than  $-1$ , so the dark energy behaves as quintessence-like. For  $\alpha < 0$ , energy is transferred from dark matter to dark energy, so the effective equation of state of dark energy crosses  $-1$ , i.e. it exhibits quintom behaviors. On the right side of Fig. 1, we plot the equation of state for fixed  $\alpha$  with different values of  $c$  ( $\alpha = -0.11$  in this particular case). As  $c$  increases, the equation of state depart from  $-1$  and increases. For large value of  $c$  the quintom divide is not crossed, and the model again behaves like a quintessence. In Fig. 2 we plot  $\rho_{\text{de}}(z)$ . On the left of Fig. 2, we plot the special case of HDE ( $\alpha = 0$ ). we find that for  $0 < c < 1$ , the equation of state will cross  $-1$  and behave like a “quintom”, so that  $\rho_{\text{HDE}}$  diverges in finite time; for  $c > 1$ , the equation of state is greater than  $-1$ , and the dark energy density decrease as time passes. On the right of Fig. 2, we plot behavior of the system with different values of  $\alpha$  with  $c = 1$ . For sufficiently negative  $\alpha$ , the IHDE density diverges as energy is transferred

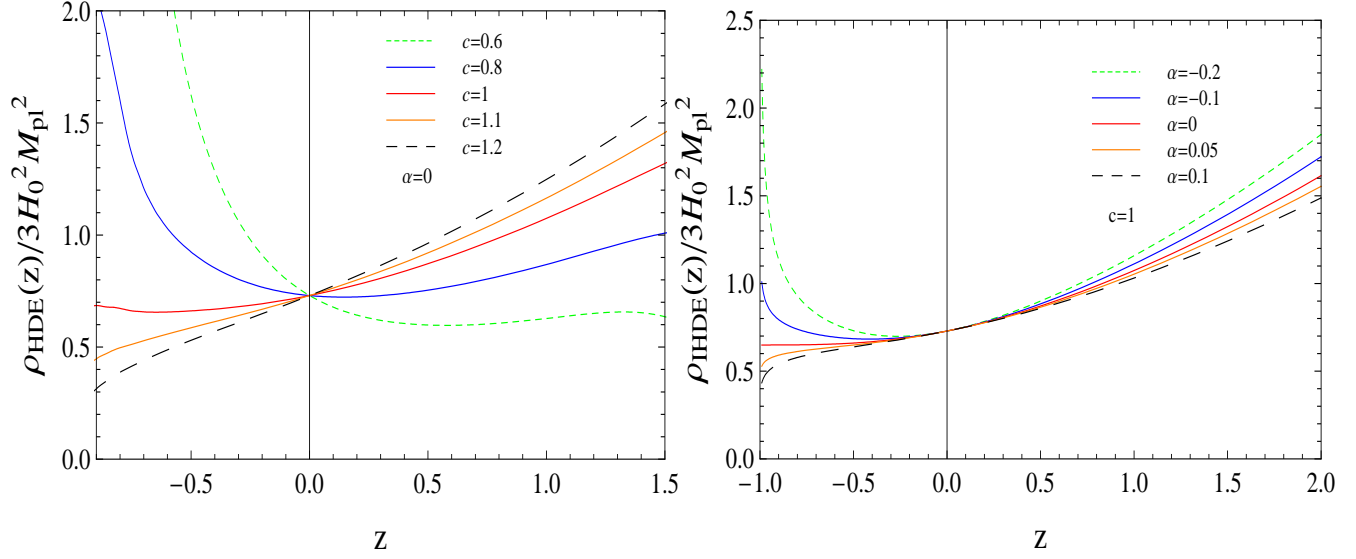


FIG. 2: Energy density of IHDE and HDE model. Left: Energy density of HDE . Right: Energy density of IHDE. Here we set  $\Omega_{m0} = 0.27$ .

from the dark matter to dark energy, and eventually we would run into the “Big Rip”.

### III. METHODOLOGY

#### A. Data analysis

We utilize several data sets to constrain the parameters of the holographic dark energy model, including a selection of 182 high-quality type Ia supernovae, the baryon acoustic oscillation measurement from the Sloan Digital Sky Survey, 42 latest X-ray gas mass fraction data from Chandra observations, 27 GRB samples generated with  $E_{peak} - E_\gamma$  correlation, and the CMB shift parameter from WMAP 3 years result.

##### 1. Selected SN Ia data set

For the SN Ia data, our sample includes 77 highest quality data from the Riess Gold 06 sample [35] (30 HST supernovae and 47 high quality SNLS supernovae [36])[48], and 105 ESSENCE supernovae [37] (60 observed by the ESSENCE team and 45 nearby supernovae re-analyzed by the ESSENCE team), the total number is 182. We use the light curve fitters MLCS2k2 [49, 50] (the other light curve fitter SALT [51] give results which are consistent



with MLCS2k2 [35, 37]), this algorithm avoids the need of normalization [52]. The redshift of this data set reaches 1.755.

The likelihood function of the parameters can be determined from  $\chi^2$  statistics, and for SN Ia data

$$\chi_{\text{SN}_{\text{sel}}}^2(\theta) = \sum_{i=1}^{182} \frac{(\mu_{\text{obs}}(z_i) - \mu_{\text{th}}(z_i))^2}{\sigma_i^2}, \quad (17)$$

where the theoretical value of distance modulus  $\mu_{\text{th}}(z)$  is given by

$$\begin{aligned} \mu_{\text{th}}(z) &= 5 \log_{10} d_L(z) + 25 \\ &= 5 \log_{10} D_L(z) - 5 \log_{10} h_0 + 42.38, \end{aligned} \quad (18)$$

and

$$D_L(z) = \frac{H_0}{c} \times d_L(z). \quad (19)$$

Here  $H_0 = 100h_0 \text{ km s}^{-1} \text{ Mpc}^{-1}$  and the luminosity distance  $d_L$  can be written as

$$d_L(z) = (1+z) \int_0^z \frac{cdz'}{H(z')}. \quad (20)$$

## 2. BAO measurement from SDSS

The baryon acoustic oscillation signatures in the large-scale clustering of galaxies can be seen as a standard ruler providing another way to explore the expansion history of the Universe. We use the measurement of the BAO peak from a spectroscopic sample of 46,748 luminous red galaxies (LRGs) observations of SDSS to test cosmology [41], which gives the value of  $A = 0.469(n_s/0.98)^{-0.35} \pm 0.017$  at  $z_{\text{BAO}} = 0.35$  where  $n_s = 0.95$  [53]. The expression of A can be written as

$$A = \frac{\sqrt{\Omega_{m0}}}{(H(z_{\text{BAO}})/H_0)^{1/3}} \left[ \frac{1}{z_{\text{BAO}}} \int_0^{z_{\text{BAO}}} \frac{dz'}{H(z')/H_0} \right]^{2/3}, \quad (21)$$

and the  $\chi_{\text{BAO}}^2$  is

$$\chi_{\text{BAO}}^2 = \left( \frac{A - 0.469(n_s/0.98)^{-0.35}}{0.017} \right)^2. \quad (22)$$

### 3. Latest X-ray gas mass fraction data from Chandra

The X-ray gas mass fraction in the largest, X-ray luminous, dynamically relaxed clusters of galaxies provides a fair sample of the matter content of the Universe. It could give a constraint to the geometry of the Universe with the relation  $f_{\text{gas}} \propto d_A^{1.5}$ , under the assumption that this fraction should be approximately constant with redshift [33, 54, 55]. Here we use the latest  $f_{\text{gas}}$  data derived from 42 relaxed clusters by Allen *et. al* [38]. from *Chandra* observations [38], the redshift of this sample ranges from 0.05 to 1.1.

Following Allen *et. al* [38], the  $\chi^2_{f_{\text{gas}}}$  is given by

$$\chi^2_{f_{\text{gas}}}(\theta) = \left( \sum_{i=1}^{42} \frac{[f_{\text{gas}}^{\Lambda\text{CDM}}(z_i) - f_{\text{gas},i}]^2}{\sigma_{f_{\text{gas},i}}^2} \right) + \left( \frac{\Omega_b h_0^2 - 0.0214}{0.0020} \right)^2 + \left( \frac{h_0 - 0.72}{0.08} \right)^2 + \left( \frac{s_0 - 0.16}{0.048} \right)^2 + \left( \frac{K - 1.0}{0.1} \right)^2 + \left( \frac{\eta - 0.214}{0.022} \right)^2, \quad (23)$$

and the model fitted to the reference  $\Lambda\text{CDM}$  ( $\Omega_{m0} = 0.3, \Omega_{\Lambda 0} = 0.7$ ) data is

$$f_{\text{gas}}^{\Lambda\text{CDM}}(z) = \frac{KA\gamma b(z)}{1 + s(z)} \left( \frac{\Omega_b}{\Omega_m} \right) \left[ \frac{d_A^{\Lambda\text{CDM}}(z)}{d_A(z)} \right]^{1.5}, \quad (24)$$

where  $d_A(z)$  and  $d_A^{\Lambda\text{CDM}}(z)$  are the angular diameter distances to the clusters in the test model and reference model,

$$d_A(z) = \frac{1}{(1+z)} \int_0^z \frac{cdz'}{H(z')}. \quad (25)$$

The parameter  $b(z) = b_0(1 + \alpha_b z)$  in Eq. (24) is the bias factor which parameterizes the redshift-dependent deviation of the baryon fraction measured at  $r_{2500}$  from the Universe mean with  $0.65 < b_0 < 1.0$ ,  $-0.1 < \alpha_b < 0.1$ ; The factor  $s(z) = s_0(1 + \alpha_s z)$  models the baryonic mass fraction in stars, and  $s_0 = (0.16 \pm 0.05)h_{70}^{0.5}$ ,  $-0.2 < \alpha_s < 0.2$ . The  $A$  accounts for the change in angle subtended by  $r_{2500}$  as the reference cosmological model is varied:

$$A = \left( \frac{\theta_{2500}^{\Lambda\text{CDM}}}{\theta_{2500}} \right)^\eta \approx \left( \frac{H(z)d_A(z)}{[H(z)d_A(z)]^{\Lambda\text{CDM}}} \right)^\eta, \quad (26)$$

and  $\eta$  is the slope of the  $f_{\text{gas}}$  in the region of  $r_{2500}$  measured in the reference  $\Lambda\text{CDM}$  model, which takes the value  $\eta = 0.214 \pm 0.022$ . The parameter  $\gamma$  represents the effect of non-thermal pressure support in the clusters, which ranges from 1.0 to 1.1; The factor  $K$  is a ‘calibration’ constant which accounts for residual uncertainty in the accuracy of the instrument calibration and X-ray modeling, and we take  $K = 1 \pm 0.1$ .

#### 4. Gamma-ray bursts data

The GRB data may be a good complement to the other observational data [39, 40, 56, 57, 58, 59, 60, 61], such as SN Ia data. They have very large redshift distribution and can be observed at much higher redshift, thus provide an effective way to detected the evolution of the dark energy.

Our GRB data set is constituted of 27 GRB samples in Ref. [39]. They are generated from the  $E_{peak} - E_\gamma$  correlation (Ghirlanda relation [40]), which is one of the tightest correlations for GRB. The redshift of this data set reaches 6.29.

The  $\chi^2_{\text{GRB}}$  takes the form of:

$$\chi^2_{\text{GRB}}(\theta) = \sum_{i=1}^{27} \frac{(\mu_{obs}(z_i) - \mu_{th}(z_i))^2}{\sigma_i^2}, \quad (27)$$

in which a distance modulus  $\mu_{obs}(z)$  estimated from the observational data can be calculated as

$$\mu_{obs}(z) = 5 \log_{10}(d_{L_{obs}}) + 25, \quad (28)$$

with a estimated luminosity distance  $d_{L_{obs}}$  expressed in unit of megaparsecs, and

$$d_{L_{obs}} = [E_\gamma(1+z)/(4\pi F_{beam} S_{bolo})]^{1/2}. \quad (29)$$

Here  $F_{beam}$  is the beaming factor,  $S_{bolo}$  is the bolometric fluence of the burst, and the collimation corrected energy  $E_\gamma$  can be fitted by

$$\log E_\gamma = a + b \log[E_{peak}(1+z)/300keV], \quad (30)$$

where  $a = 50.57$  and  $b = 1.63$ . Its uncertainty is

$$\sigma_{\log E_\gamma}^2 = \sigma_a^2 + (\sigma_b \log[E_{peak}(1+z)/300keV])^2 + (0.4343b\sigma_{E_{peak}}/E_{peak})^2 + \sigma_{E_\gamma,sys}^2, \quad (31)$$

where the  $1\sigma$  uncertainties in the intercept and slope are  $\sigma_a = 0.09$  and  $\sigma_b = 0.03$ , and the best estimated  $\sigma_{E_\gamma,sys}$  is 0.16. The  $\sigma_i$  in Eq. (27) can be estimated as

$$\sigma_i = [(2.5\sigma_{\log E_\gamma})^2 + (1.086\sigma_{S_{bolo}}/S_{bolo})^2 + (1.086\sigma_{F_{beam}}/F_{beam})^2]^{1/2}. \quad (32)$$

At last, the expression of  $\mu_{th}(z)$  in Eq. (27) is given by Eq. (18).

### 5. CMB shift parameter from WMAP 3 years result

The shift parameter is a very good complement to the previous data set because the very large redshift distribution ( $z_{\text{CMB}} = 1089$ ) can reflect the evolution of the dark energy. The shift parameter  $R$  is derived from the CMB data takes the form as

$$R = \sqrt{\Omega_{\text{m}0}} \int_0^{z_{\text{CMB}}} \frac{dz'}{H(z')/H_0}. \quad (33)$$

The WMAP3 data gives  $R = 1.70 \pm 0.03$  [62], thus we have

$$\chi_{\text{CMB}}^2 = \left( \frac{R - 1.70}{0.03} \right)^2. \quad (34)$$

To break the degeneracy and explore the power and differences of the constraints for these data sets, we use them in several combinations to perform our fitting:  $\text{SN}_{\text{sel}} + \text{BAO}$ ,  $\text{SN}_{\text{sel}} + \text{BAO} + f_{\text{gas}}$ , and  $\text{SN}_{\text{sel}} + \text{BAO} + f_{\text{gas}} + \text{GRB} + \text{CMB}$ .

## B. MCMC

Markov Chain Monte Carlo (MCMC) techniques are widely used to generate random samples to simulate the posterior probability of the parameters given the data sets. This method has several advantages over grid-based approach. Most importantly, the computational time cost increases approximately linearly with the number of parameters, so even for a large number of parameters the estimate can be done within an acceptable computation time [63, 64, 65, 66].

We use the Metropolis-Hastings algorithm with uniform prior to decide whether to accept a new point into the chain by an acceptance probability:

$$\mathbf{a}(\theta_{\mathbf{n}+1}|\theta_{\mathbf{n}}) = \min \left\{ \frac{\mathbf{p}(\theta_{\mathbf{n}+1}|\mathbf{d}) \mathbf{q}(\theta_{\mathbf{n}}|\theta_{\mathbf{n}+1})}{\mathbf{p}(\theta_{\mathbf{n}}|\mathbf{d}) \mathbf{q}(\theta_{\mathbf{n}+1}|\theta_{\mathbf{n}})}, 1 \right\},$$

where  $\mathbf{p}(\theta)$  is the prior probability distribution and  $\mathbf{q}(\theta_{\mathbf{n}+1}|\theta_{\mathbf{n}})$  is the proposal density of proposing a new point  $\theta_{\mathbf{n}+1}$  given a current point  $\theta_{\mathbf{n}}$  in the chain. If  $\mathbf{a} = 1$ , the new point  $\theta_{\mathbf{n}+1}$  is accepted; otherwise, the new point is accepted with probability  $\mathbf{a}$ . The trials are repeated until a new point is accepted, and then we set  $\theta_{\mathbf{n}} = \theta_{\mathbf{n}+1}$ . In our computation, we set a Gaussian-distributed proposal density for every point which is independent of the

position on the chain, so that  $\mathbf{q}(\theta_{n+1}|\theta_n)$  and  $\mathbf{q}(\theta_n|\theta_{n+1})$  are canceled, and consider the uniform prior and Bayes' theorem we get

$$\mathbf{a}(\theta_{n+1}|\theta_n) = \min \left\{ \frac{\mathcal{L}(\mathbf{d}|\theta_{n+1})}{\mathcal{L}(\mathbf{d}|\theta_n)}, 1 \right\}. \quad (35)$$

Here  $\mathcal{L}(\mathbf{d}|\theta)$  is the likelihood to obtain the data set  $\mathbf{d}$  given the parameter set  $\theta$ , and usually can be written as

$$\mathcal{L}(\mathbf{d}|\theta) = \frac{1}{\sqrt{2\pi}\sigma_{\mathbf{d}}} e^{-\frac{1}{2}\chi^2}. \quad (36)$$

For our three data sets, the  $\chi^2$  are

$$\chi^2 = \begin{cases} \chi_{\text{SN}_{\text{sel}}}^2 + \chi_{\text{BAO}}^2 \\ \chi_{\text{SN}_{\text{sel}}}^2 + \chi_{\text{BAO}}^2 + \chi_{\text{f}_{\text{gas}}}^2 \\ \chi_{\text{SN}_{\text{sel}}}^2 + \chi_{\text{BAO}}^2 + \chi_{\text{f}_{\text{gas}}}^2 + \chi_{\text{GRB}}^2 + \chi_{\text{CMB}}^2, \end{cases} \quad (37)$$

respectively. We assume uniform prior for the parameters of our models within the given ranges as following:  $\Omega_{m0} \in (0, 1)$ ,  $c \in (0, 2)$ ,  $\alpha \in (-0.2, 0.2)$  and  $h_0 \in (0.4, 0.9)$ . In particular, when we use  $\text{f}_{\text{gas}}$  data, the parameters coming from this data set  $\theta_{\text{data}} = \{ \Omega_b, s_0, \alpha_s, b_0, \alpha_b, \eta, \gamma, K \}$ , are also included in our MCMC fitting process.

The thermodynamical bound  $c > \sqrt{\Omega_D}$  is NOT assumed *a priori*, as we wish to assess the value of the data fairly.

We generate six chains for each case we study, and about one hundred thousand points are sampled in each chain. The form of proposal density we use is described in Ref. [67]. After the convergence determined by Gelman and Rubin [68] criterion and thinning the chains, we merge them into one chain which consists of about 10,000 points used to simulate the probability distribution of the parameters.

### C. Model Comparison

For comparing different models, one must choose a statistical variable, the  $\chi_{\text{min}}^2$  is the simplest one and is widely used. However, for models with different number of parameters, the comparison using  $\chi^2$  may not be fair, as one would expect that models with more parameters tends to have lower  $\chi^2$ .

The Akaike information criterion (AIC) [69]

$$\text{AIC} = -2 \ln \mathcal{L}_{\text{max}} + 2k \quad (38)$$

includes the penalization of the number of parameters, where  $\mathcal{L}_{max}$  is the maximum likelihood and  $k$  is the number of parameters [70, 71]. However, the size of the data is not embodied in the AIC, if there is a large number of data, then the reduction in  $\chi^2$  due to the additional parameters may be very large and the  $2k$  term in the AIC smaller could not compensate it [72].

The Bayesian information criterion(BIC) [73] can be written as

$$\text{BIC} = -2 \ln \mathcal{L}_{max} + k \ln N, \quad (39)$$

where  $N$  is the number of data. The BIC tends to penalize the number of parameters too much if given large number of data [71, 72, 74].

We will use the Bayesian evidence (BE) as a model selection criterion. The Bayesian evidence of a model  $M$  takes the form

$$\text{BE} = \int \mathcal{L}(\mathbf{d}|\theta, M) \mathbf{p}(\theta|M) d\theta, \quad (40)$$

where  $\mathcal{L}(\mathbf{d}|\theta, M)$  is the likelihood function given the model  $M$  and parameters  $\theta$ , and  $\mathbf{p}(\theta|M)$  is the priors of parameters. The BE may be the best model selection criterion, as it is the average of likelihood of a model over its prior of the parameter space and automatically includes the penalties of the number of parameters and data, so it is more direct, reasonable and unambiguous than the  $\chi^2_{min}$ , AIC and BIC in model selection [70, 75, 76, 77, 78, 79, 80, 81] (For a connection between BE and  $\chi^2_{min}$  analysis, see Ref. [82]). The logarithm of BE can be used as a guide for model comparison (Jeffreys 1961), and we choose the  $\Lambda$ CDM as the reference model:  $\Delta \ln \text{BE} = \ln \text{BE}_{model} - \ln \text{BE}_{\Lambda\text{CDM}}$ . The strength of the evidence for the model is considered according to the numerical value of BE:

$$\left\{ \begin{array}{ll} \Delta \ln \text{BE} < 1 & \text{Weak} \\ 1 < \Delta \ln \text{BE} < 2.5 & \text{Significant} \\ 2.5 < \Delta \ln \text{BE} < 5 & \text{Strong to very strong} \\ \Delta \ln \text{BE} > 5 & \text{Decisive} \end{array} \right. \quad (41)$$

We use the nested sampling technique to compute BE [78, 83].

## IV. RESULTS

### A. The HDE Model

In Table I, we give the best fit value and the  $1\sigma$  error of the HDE model parameters, as well as the value of  $\ln \Delta \text{BE}$  for the three data set combinations. We plot the probability distribution function (PDF) of the HDE model in Fig. 3. We can see that the best fit of  $\Omega_{m0}$  are almost the same (around 0.27) for all data sets. The best fit of  $c$  varies slightly across the different data sets, it is 0.761 for the SN+BAO data set, but decreases slightly when the  $f_{\text{gas}}$ , GRB and CMB data are included. However, for all data sets, we have  $c < 1$  at more than  $1.5\sigma$  (see Fig. 3). The PDF of the parameter distribution is smoothly distributed.

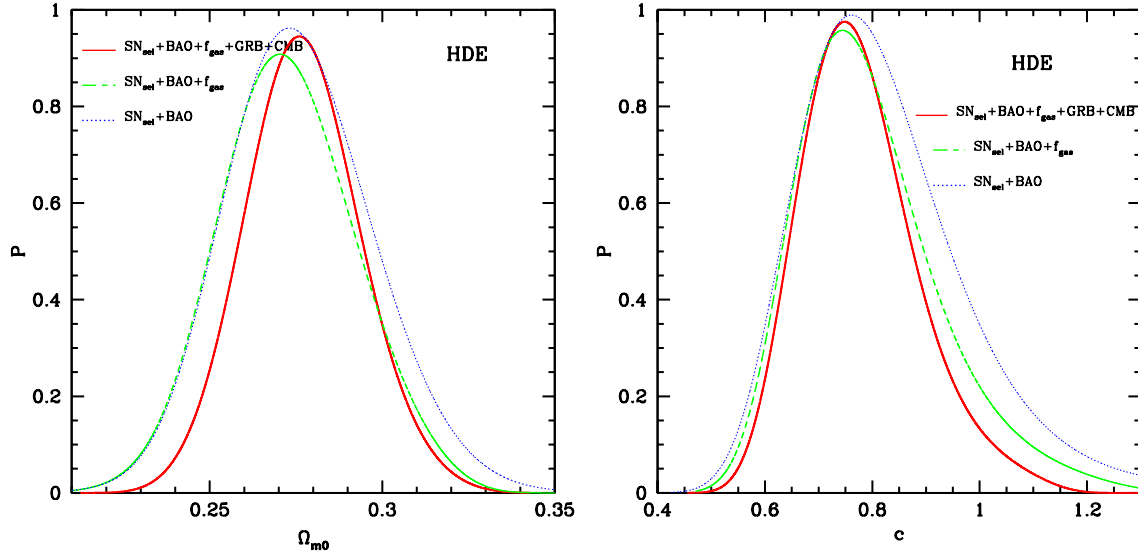


FIG. 3: Probability distribution function (PDF) of the parameters for the fits of HDE model. Left: The PDF for parameter  $\Omega_{m0}$ . Right: The PDF for parameter  $c$ .

TABLE I: The fitting result for the HDE model

	SN + BAO	SN + BAO + $f_{\text{gas}}$	SN + BAO + $f_{\text{gas}}$ + GRB + CMB
$\Omega_{m0}$	$0.273^{+0.020}_{-0.020}$	$0.270^{+0.021}_{-0.018}$	$0.276^{+0.017}_{-0.016}$
$c$	$0.761^{+0.154}_{-0.117}$	$0.745^{+0.130}_{-0.101}$	$0.748^{+0.108}_{-0.093}$
$\Delta \ln \text{BE}$	$0.09 \pm 0.12$	$0.63 \pm 0.18$	$0.65 \pm 0.18$

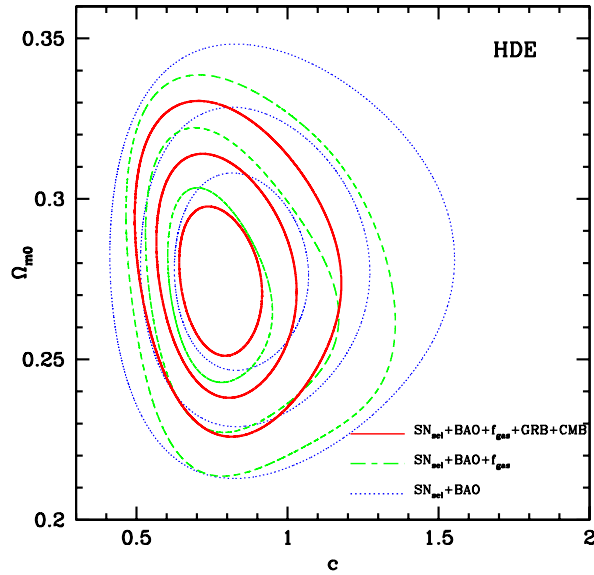


FIG. 4: The contour maps of  $c$  vs.  $\Omega_{m0}$  for HDE with  $1\sigma(68.3\%)$ ,  $2\sigma(95.5\%)$  and  $3\sigma(99.7\%)$  confidence levels.

The parameter  $c$  plays an essential role in determining the evolution of the HDE model. If  $c = 1$ , the dark energy equation of states would asymptote to that of a cosmological constant and the Universe would enter the de Sitter phase in the future; if  $c > 1$ , the equation of state of dark energy would always be greater than  $-1$ , it would behave as quintessence dark energy; if  $c < 1$ , initially the equation of state of HDE would be greater than  $-1$ , but it would decrease and eventually cross the “phantom divide line” ( $w = -1$ ) as the Universe expands, acting as a quintom [84].

We plot the contour maps of  $c$  vs.  $\Omega_{m0}$  for HDE with  $1\sigma(68.3\%)$ ,  $2\sigma(95.5\%)$  and  $3\sigma(99.7\%)$  confidence levels in Fig. 4. Our constraint is tighter than previous ones, e.g. Ref. [30], as we have used more precise data in our fitting. The center of the best fit is located at  $c < 1$ , but there is still a fair fraction of allowed parameter space in which  $c > 1$ . The evolution of  $w$  and  $\rho_{de}$  in HDE models with the best fit parameters for the three data set combinations are shown in Fig. 5. For these cases, as we expected, the dark energy diverges in finite time and the Universe ends with a Big Rip.

Moreover, for all the four data sets, we have  $c < 1.2$  at more than  $3\sigma$  (see Fig. 3 and Fig. 4), which is rather consistent with the possible theoretical limit of parameter  $c$  from the weak gravity conjecture (see [23]).



The HDE model fits about equally well ( $\ln \text{BE}=0.09$ ) as the  $\Lambda\text{CDM}$  when we only use the SNIa and BAO data. With  $f_{\text{gas}}$ , GRB and CMB data added, it fits mildly better than the  $\Lambda\text{CDM}$ , but with the data presently available the difference is not significant ( $\ln \text{BE}=0.63 \sim 0.65$ ).

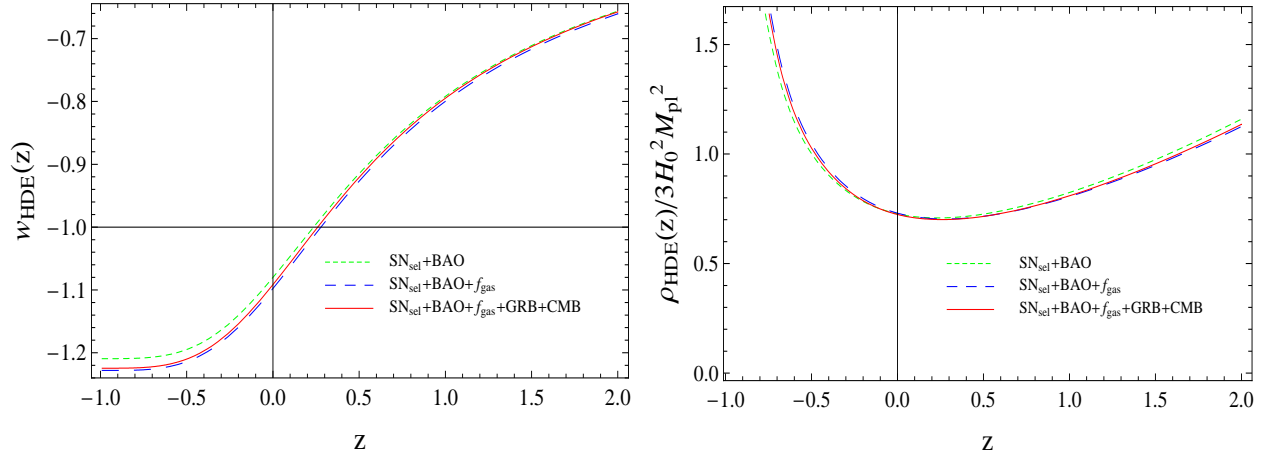


FIG. 5: Evolution of the dark energy in the best fit HDE model. Left: Equation of state. Right: Dark energy density.

## B. The IHDE Model

TABLE II: The Fitting results the IHDE model

	SN + BAO	SN + BAO + $f_{\text{gas}}$	SN + BAO + $f_{\text{gas}}$ + GRB + CMB
$\Omega_{m0}$	$0.272^{+0.023}_{-0.022}$	$0.275^{+0.021}_{-0.021}$	$0.281^{+0.017}_{-0.017}$
$c$	$0.592^{+0.204}_{-0.113}$	$0.667^{+0.321}_{-0.164}$	$0.692^{+0.135}_{-0.107}$
$\alpha$	$-0.020^{+0.145}_{-0.174}$	$0.068^{+0.093}_{-0.120}$	$-0.006^{+0.021}_{-0.024}$
$\Delta \ln \text{BE}$	$0.41 \pm 0.12$	$0.70 \pm 0.18$	$0.75 \pm 0.18$

In Table II, we give the best fit value and the  $1\sigma$  error of the IHDE model parameters, as well as the value of  $\ln \Delta \text{BE}$  for the three data set combinations. We plot the probability distribution function (PDF) of the IHDE model in Fig. 6. We also plot the  $\Omega_{m0} - c$  contours in Fig. 7. The evolution of the effective equation of state and the relative density of the

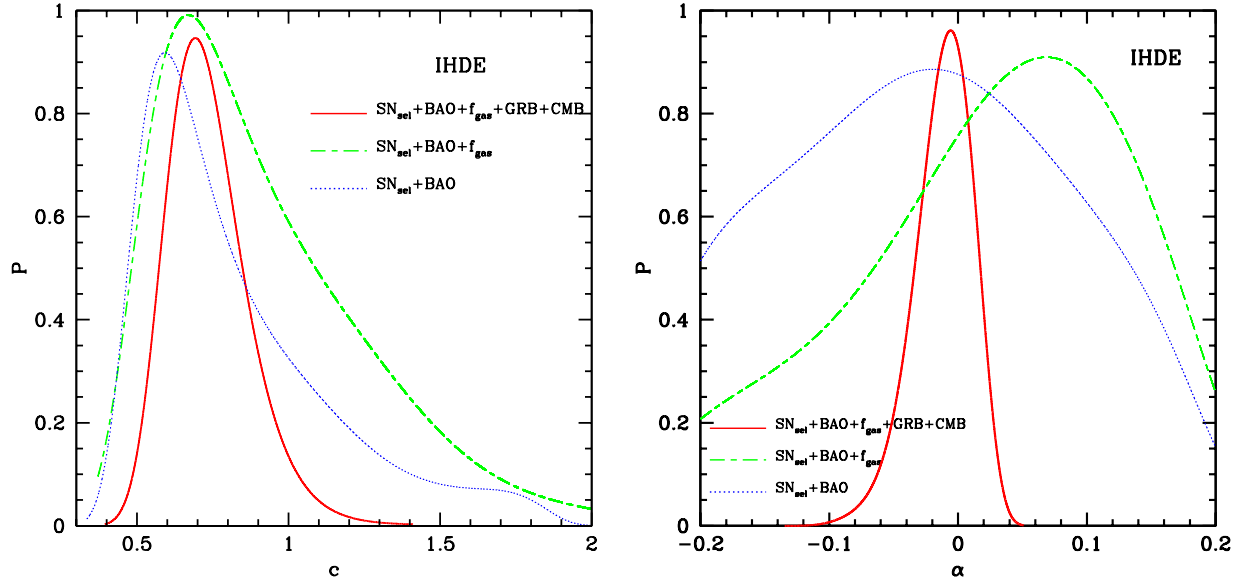


FIG. 6: The PDF of the parameters for the fits of IHDE model. Left: The PDF for parameter  $c$ . Right: The PDF for parameter  $\alpha$ .

dark energy are plotted in Fig. 8. Similar to the case of HDE models, the best fit of  $\Omega_{m0}$  for the IHDE models is around 0.27–0.28 for all three data set combinations, as can be seen from Fig. 7. However, for the different data set combinations, the distribution of  $c$  and  $\alpha$  are fairly different (see Fig. 6 and Table II). The peaks of the PDF for  $\alpha$  are different for the three data set combinations. Furthermore, the evolution of the equation of state for the three data set combinations are also very different (see Fig. 8).

Does this mean that the three different data sets indicate very different expansion behavior? If so, this would indicate that the three data sets may be inconsistent with each other. However, we have seen that for the case of HDE the three different data set combinations yield similar fitting parameters, indicating that they are basically consistent with each other.

To understand the origin of this difference, we plot the expansion rate in Fig. 9 for the best fit model parameters of the three data set combinations. While there are differences, one can see qualitatively the three set of curves are similar to each other. This shows that the different data sets are not inconsistent.

The reason of the difference seems to be due to parameter degeneracy in the IHDE model. In this model, we have two parameters  $c$  and  $\alpha$ , it appears that different combination of

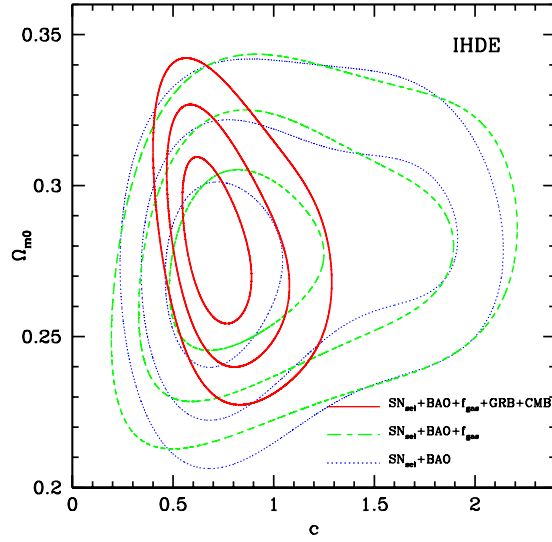


FIG. 7: The contour maps of  $c$  vs.  $\Omega_{m0}$  for IHDE with  $1\sigma$ (68.3%),  $2\sigma$ (95.5%) and  $3\sigma$ (99.7%) confidence levels.

these two parameters may lead to similar dynamical behavior. At first sight, this seems to be in disagreement with our analysis in §2, where the effective equation of state  $w_{\text{eff}}$  of the dark energy was given in terms of these two parameters. However, the equation of state  $w_{\text{eff}}$  of the dark energy is not the only thing affecting the expansion. In this model, the interaction between dark matter and dark energy induces a non-zero effective equation of state for the dark matter. Thus, although the effective equation of state for the dark energy looks very different, the change in the dark matter equation of state compensates part of this

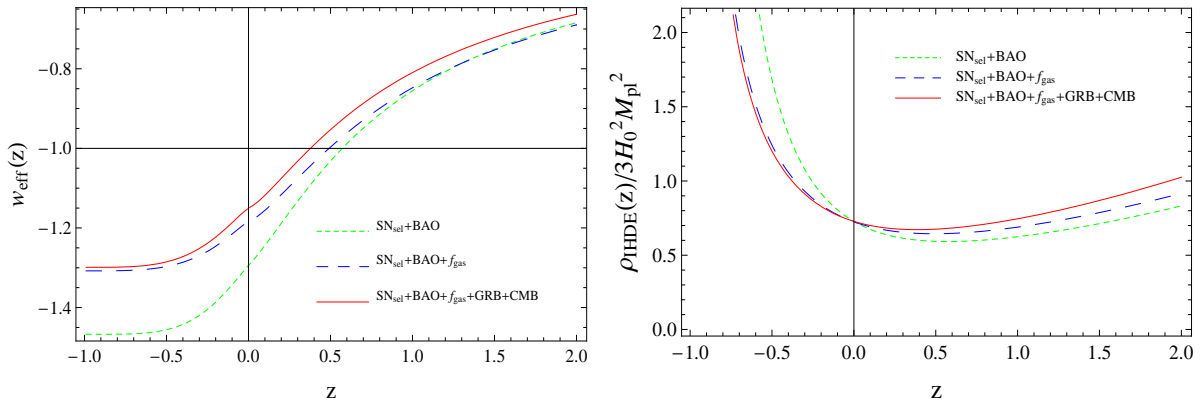


FIG. 8: Effective equation of state and density evolution for the best fit IHDE models.

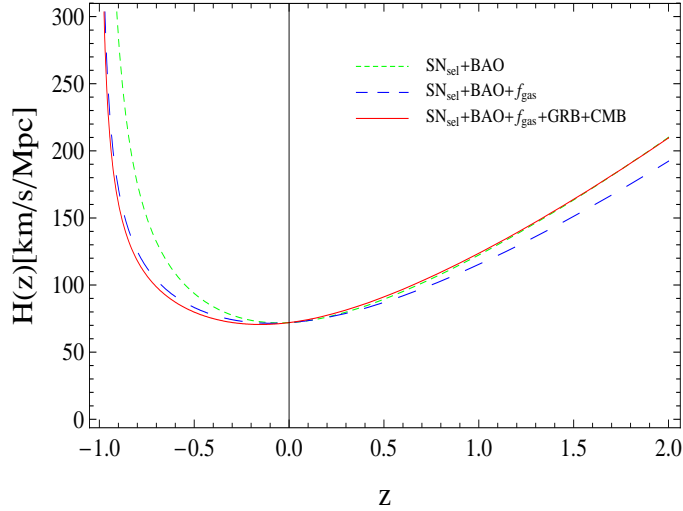


FIG. 9: The expansion rate  $H(z)$  for the best fit parameters of the IHDE model.

difference. Further, this model still has some shortcomings since  $\Omega_{de}$  could quantitatively evolve to region larger than 1 if  $\alpha < 0$ , i.e. if dark matter decays into dark energy, because the interaction term does not concern the energy density of dust matter [47]. At this case,

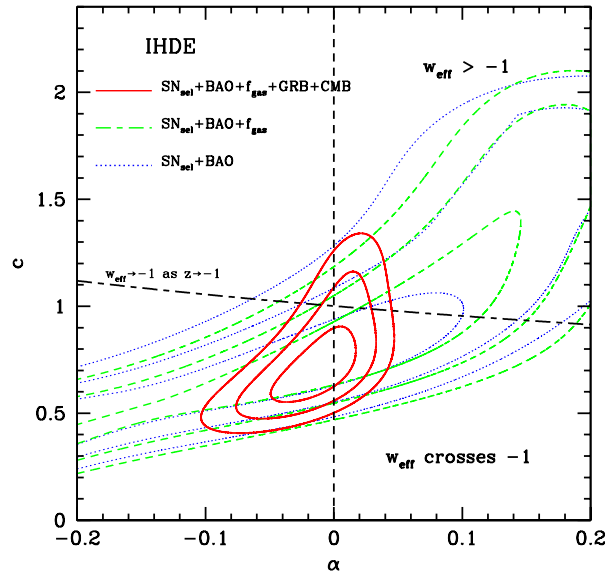


FIG. 10: The contour maps of  $\alpha$  vs.  $c$  for IHDE with  $1\sigma(68.3\%)$ ,  $2\sigma(95.5\%)$  and  $3\sigma(99.7\%)$  confidence levels. The black dot-dashed curve denotes  $w_{\text{eff}} = -1$  when  $z \rightarrow -1$  with  $\Omega_{\text{IHDE}0} = 0.73$ , and the region below (over) it means  $w_{\text{eff}}$  will (not) cross -1 during finite time.

the IHDE model is only effective in the period prior to the Big Rip. We will improve our work and discuss the possible interaction forms in the next several papers.

The contour map for  $c$  and  $\alpha$  is plotted in Fig. 10. From the Fig, the contours corresponding to the data sets SN+BAO+ $f_{gas}$ +GRB+CMB are much tighter than the other data sets. This is because we use the data set GRB and CMB, which has very large redshift distribution so they break the degeneracy of the parameter  $c$  and  $\alpha$ . We also mark the  $\alpha - c$  values for which  $w_{eff} = -1$  as a dashed line. This forms the dividing line between quintessence-like and phantom-like behavior. For the best fit parameters of all three data set combinations,  $c \sim 0.6 < 1$ . The value of  $\alpha$  varies more, but all consistent with being 0 within  $1.5\sigma$ , there is no strong evidence for the presence of interaction. For the SN+BAO+ $f_{gas}$ +GRB+CMB, the PDF of parameter  $\alpha$  and the best fit values strongly suggest the evidence for the interaction is very weak. In any case, for all three data set combinations, the best fit value resides in the phantom-like region, although a large area of quintessence-like region is also allowed.

The IHDE model is mildly favored over the  $\Lambda$ CDM model according to the BE criterion, the evidence is slightly stronger than the HDE model case, but not yet sufficient for drawing strong conclusions.

## V. CONCLUSION

In this paper we firstly gave a brief review of holographic dark energy model for both the non-interacting case and interacting case. We introduced a new interacting term  $Q = 3\alpha H\rho_{de}$  and the non-interacting case could be viewed as the special case with  $\alpha = 0$ . We derived the equations for the evolution of  $\Omega_{de}$  and  $H(z)$ , and illustrated the dynamical behavior of these models by chosen some representative values of the parameters  $c$  and  $\alpha$ . The condition for the model to have “Big Rip” is determined.

Secondly, we utilize several data sets from the resent observations to constrain the models. Our data sets consist of the selected 182 high-quality type Ia supernovae, the baryon acoustic oscillation measurement from the Sloan Digital Sky Survey, the latest X-ray gas mass fraction data from *Chandra* observations, 27 GRB samples generated with  $E_{peak} - E_\gamma$  correlation, and the CMB shift parameter from WMAP three years result. We used the MCMC technique to simulate the posterior probability of the model parameters. The best-fits for the three data sets are given in Table 1 for the HDE model, and Table 2 for the IHDE model. We

also give the probability distribution of the parameters and the contour maps for the HDE and IHDE models.

Next, we utilize the Bayesian evidence (BE) as a model selection criterion to compare the holographic models with  $\Lambda$ CDM model for the three data sets. The BE is particularly appropriate for comparing models with different number of parameters. Both the HDE and the IHDE model are mildly favored by the current observational data set, although the evidence is weak. For both the HDE and IHDE models, the data favors “quintom” behavior slightly, i.e. the dark energy initially has  $w_{eff} > -1$ , but eventually crossing the phantom dividing line, and the model ends with a “Big Rip”. However, quintessence-like behavior is also still allowed with the present data.

In brief, we conclude that according to the combined measurements data, the holographic dark energy model, especially the interacting holographic dark energy model is mildly favored by the observations, and for the best fit model the equation of state for both the HDE and IHDE crosses  $-1$ , for which the Universe ends up in a Big Rip.

### Acknowledgements

We would like to thank Bin Wang, Chunshan Lin, Feng-Quan Wu, Hao Wei, Miao Li, Rong-Gen Cai, Steven Allen, Xin Zhang, Yi Wang and Yungui Gong for helpful discussions. One of the authors (Yin-Zhe Ma) also thanks Hao Yin, Jian Ma and Nan Zhao for the help of computer program. Yin-Zhe Ma and Xuelei Chen thank “UCLA 2008 dark matter and dark energy” advisory committee at Los Angeles for hospitality during their stay when they present their work on the symposium. Our MCMC chain computation was performed on the Supercomputing Center of the Chinese Academy of Sciences and the Shanghai Supercomputing Center. This work is supported by the National Science Foundation of China under grants 10525314, 10325525, 90403029 and 10525060, the Key Project Grant 10533010, by the Chinese Academy of Sciences under grant KJCX3-SYW-N2, and by the Ministry of Science and Technology under the national basic sciences program (973) under grant 2007CB815401.

- 
- [1] A. G. Riess *et al.* [Supernova Search Team Collaboration], *Astron. J.* **116**, 1009 (1998) [astro-ph/9805201]; S. Perlmutter *et al.* [Supernova Cosmology Project Collaboration], As-

- trophys. J. **517**, 565 (1999) [astro-ph/9812133].
- [2] M. Tegmark *et al.* [SDSS Collaboration], Phys. Rev. D **69**, 103501 (2004) [astro-ph/0310723];
- [3] D. N. Spergel *et al.* [WMAP Collaboration], Astrophys. J. Suppl. **148**, 175 (2003) [astro-ph/0302209]; D. N. Spergel *et al.*, astro-ph/0603449.
- [4] P. J. Steinhardt, in *Critical Problems in Physics*, edited by V. L. Fitch and D. R. Marlow (Princeton University Press, Princeton, NJ, 1997).
- [5] E. Witten, hep-ph/0002297.
- [6] A. G. Cohen, D. B. Kaplan and A. E. Nelson, Phys. Rev. Lett. **82**, 4971 (1999) [hep-th/9803132].
- [7] P. Horava and D. Minic, Phys. Rev. Lett. **85**, 1610 (2000) [hep-th/0001145]; S. D. Thomas, Phys. Rev. Lett. **89**, 081301 (2002).
- [8] S. D. H. Hsu, Phys. Lett. B **594**, 13 (2004) [hep-th/0403052].
- [9] M. Li, Phys. Lett. B **603**, 1 (2004) [hep-th/0403127].
- [10] G. 't Hooft, gr-qc/9310026; L. Susskind, J. Math. Phys. **36**, 6377 (1995) [hep-th/9409089].
- [11] J. D. Bekenstein, Phys. Rev. D **7** (1973) 2333; J. D. Bekenstein, Phys. Rev. D **9** (1974) 3292; J. D. Bekenstein, Phys. Rev. D **23** (1981) 287; J. D. Bekenstein, Phys. Rev. D **49** (1994) 1912; S. W. Hawking, Commun. Math. Phys. **43** (1975) 199; S. W. Hawking, Phys. Rev. D **13** (1976) 191.
- [12] Q. G. Huang and M. Li, JCAP **0408**, 013 (2004) [astro-ph/0404229].
- [13] K. Enqvist and M. S. Sloth, Phys. Rev. Lett. **93**, 221302 (2004) [hep-th/0406019].
- [14] K. Ke and M. Li, Phys. Lett. B **606**, 173 (2005) [hep-th/0407056].
- [15] Q. G. Huang and M. Li, JCAP **0503**, 001 (2005) [hep-th/0410095].
- [16] X. Zhang, Int. J. Mod. Phys. D **14**, 1597 (2005) [astro-ph/0504586]; X. Zhang, Phys. Lett. B **648**, 1 (2007) [astro-ph/0604484]; X. Zhang, Phys. Rev. D **74**, 103505 (2006) [astro-ph/0609699].
- [17] D. Pavon and W. Zimdahl, Phys. Lett. B **628**, 206 (2005) [gr-qc/0505020].
- [18] B. Wang, Y. g. Gong and E. Abdalla, Phys. Lett. B **624**, 141 (2005) [hep-th/0506069].
- [19] H. Kim, H. W. Lee and Y. S. Myung, Phys. Lett. B **632**, 605 (2006) [gr-qc/0509040].
- [20] S. Nojiri and S. D. Odintsov, Gen. Rel. Grav. **38**, 1285 (2006) [hep-th/0506212].
- [21] B. Hu and Y. Ling, Phys. Rev. D **73**, 123510 (2006) [hep-th/0601093].
- [22] B. Chen, M. Li and Y. Wang, Nucl. Phys. B **774**, 256 (2007) [arXiv:astro-ph/0611623]; J.

- Zhang, X. Zhang and H. Liu Phys. Lett. B **651**, 84 (2007) [astro-ph/07061185]; J. Zhang, X. Zhang, H. Liu, 0708.3121 [astro-ph]
- [23] Y. Z. Ma and X. Zhang, Phys. Lett. B **661**, 239 (2008), 0709.1517 [astro-ph]
- [24] Q. G. Huang and Y. G. Gong, JCAP **0408**, 006 (2004) [astro-ph/0403590].
- [25] K. Enqvist, S. Hannestad and M. S. Sloth, JCAP **0502**, 004 (2005) [astro-ph/0409275].
- [26] J. Y. Shen, B. Wang, E. Abdalla and R. K. Su, Phys. Lett. B **609**, 200 (2005) [hep-th/0412227].
- [27] H. C. Kao, W. L. Lee and F. L. Lin, Phys. Rev. D **71**, 123518 (2005) [astro-ph/0501487].
- [28] Z. Chang, F. Q. Wu and X. Zhang, Phys. Lett. B **633**, 14 (2006) [astro-ph/0509531].
- [29] Z. L. Yi and T. J. Zhang, Mod. Phys. Lett. A **22**, 41 (2007) [astro-ph/0605596].
- [30] X. Zhang and F. Q. Wu, Phys. Rev. D **72**, 043524 (2005) [astro-ph/0506310]; X. Zhang, F. Q. Wu, Phys. Rev. D **76**, 023502 (2007) [astro-ph/0701405]
- [31] B. Wang, C. Y. Lin, E. Abdalla, Phys. Lett. B **637**, 357 (2006) [hep-th/0509107]
- [32] Q. Wu, Y. Gong, A. Wang, J. S. Alcaniz, 0705.1006 [astro-ph]
- [33] C. Feng, B. Wang, Y. Gong, R. K. Su, accepted for publication in JCAP, 0706.4033 [astro-ph]
- [34] R. R. Caldwell, M. Kamionkowski, N. N. Weinberg, Phys. Rev. Lett. **91**, 071301 (2003).
- [35] A. G. Riess et al., Astrophys. J. **656**, (2007) [astro-ph/0611572]
- [36] P. Astier et al., Astron. Astrophys. **447**, (2006) [astro-ph/0510447]
- [37] W. M. Wood-Vasey et al., (2007) [astro-ph/0701041]
- [38] S.W. Allen *et al.* 0706.0033, [astro-ph]
- [39] B. E. Scheafer, Astrophys. J. **660**, 16 (2007) [astro-ph/0612285]
- [40] G. Ghirlanda et al., Astrophys. J. Lett. **613**, L13 (2004) [astro-ph/0408350]
- [41] D. J. Eisenstein et al., Astrophys. J. **633**, 560-574 (2005) [astro-ph/0501171]
- [42] P. G. Ferreira and M. Joyce, Phys. Rev. D **58**, 023503 (1998) [astro-ph/9711102]; A. Berera and L. Z. Fang, Phys. Rev. Lett. **74**, 1912 (1995) [astro-ph/9501024]; M. Bellini, Class. Quantum Grav. **16**, 2393 (1999) [gr-qc/9904072].
- [43] A. P. Billyard and A. A. Coley, Phys. Rev. D **61**, 083503 (2000) [astro-ph/9908224]
- [44] C. Eckart, Phys. Rev. **58**, 919 (1940).
- [45] C. G. Boehmer et al., arXiv:0801.1565
- [46] K. Karwan, arXiv:0801.1755
- [47] M. Li, C. Lin and Y. Wang, arXiv:0801.1407
- [48] S. Nesseris and L. Perivolaropoulos, JCAP. **0702**, 025 (2007) [astro-ph/0612653]



- [49] A. G. Riess, W. H. Press and R. P. Kirshner, *Astrophys. J.* **473**, 88 (1996) [astro-ph/9604143]
- [50] S. Jha, A. G. Riess, R. P. Kirshner, *Astrophys. J.* **659**, 122-148 (2007) [astro-ph/0612666]
- [51] J. Guy, P. Astier, S. Nobili, N. Regnault and R. Pain, *A&A* (2005) [astro-ph/0506583]
- [52] T. M. Davis et al. (2007) [astro-ph/0701510]
- [53] D. N. Spergel et al., *Astrophys. J. Suppl. Ser.* **170**, 377 (2007) [astro-ph/0601133]
- [54] S.W. Allen et al., *Mon. Not. R. Astron. Soc.* **334**, L11-L15 (2002)
- [55] S.W. Allen et al. *Mon. Not. R. Astron. Soc.* **353**, 457-467 (2004)
- [56] E. Liang and B. Zhang, *Astrophys. J.* **633**, 611-623 (2005) [astro-ph/0504404]
- [57] G. Ghirlanda, G. Ghisellini and C. Firmani, *New J.Phys.* **8**, 123 (2006) [astro-ph/0610248]
- [58] Z. G. Dai, E. W. Liang and D. Xu, *Astrophys.J.* **612** L101-L104 (2004) [astro-ph/0407497]
- [59] D. Xu, Z. G. Dai and E. W. Liang, *Astrophys. J.* **633**, 603-610 (2005) [astro-ph/0501458]
- [60] C. Firmani, G. Ghisellini, G. Ghirlanda and V. Avila-Reese, *Mon. Not. R. Astron. Soc.* **360**, LL1 (2005) [astro-ph/0501395]
- [61] D. Hooper and S. Dodelson, *Astropart. Phys.* **27**, 113-118 (2007) [astro-ph/0512232]
- [62] Y. Wang and P. Mukherjee, astro-ph/0703780
- [63] A. Lewis and S. Bridle, *Phys. Rev. D* **66**, 103511 (2002) [astro-ph/0205436]
- [64] D. J. C. MacKay, *Information Theory, Inference, and Learning Algorithms* (2003)
- [65] R. M. Neil, *Probabilistic Inference Using Markov Chain Monte Carlo Methods* (1993)
- [66] L. Perotto et al., *JCAP.* **0610**, 013 (2006)
- [67] Y. Gong and X. L. Chen, *Phys. Rev. D* **76**, 123007, 0708.2977 [astro-ph]
- [68] A. Gelman and D. Rubin, *Statistical Science* **7**, 457 (1992).
- [69] H. Akaike, *IEEE Trans. Auto. Control* **19**, 716 (1974).
- [70] A. R. Liddle, P. Mukherjee, D. R. Parkinson, *A&G* **47** 4.30-4.33 (2006)
- [71] M. Biesiada, *JCAP.* **0702**, 003 (2007) [astro-ph/0701721]
- [72] A. R. Liddle, *Mon. Not. R. Astron. Soc.* **351**, L49-53 (2004) [astro-ph/0401198]
- [73] G. Schwarz, *Annals of Statistics* **6**, 461-464 (1978)
- [74] A. Kurek and M. Szydlowski, (2007) [astro-ph/0702484]
- [75] A. R. Liddle, (2006) [astro-ph/0701113]
- [76] M. V. John and J. V. Narlikar, *Phys. Rev. D* **65**, 043506 (2002) [astro-ph/0111122]
- [77] R. Trotta, *Mon. Not. R. Astron. Soc.* **378**, 72-82 (2007) [astro-ph/0504022]
- [78] P. Mukherjee, D. R. Parkinson and A. R. Liddle, *Astrophys.J.* **638** L51-L54 (2006)

[astro-ph/0508461]

- [79] P. Mukherjee, D. R. Parkinson, P. S. Corasaniti, A. R. Liddle and M. Kunz, MNRAS, **369** (2006) [astro-ph/0512484]
- [80] M. Kunz, R. Trotta and D. R. Parkinson, Phys. Rev. D **74**, 023503 (2006) [astro-ph/0602378]
- [81] R. Trotta (2007) [astro-ph/0703063]
- [82] P. Marshall, N. Rajguru and A. Slosar, Phys.Rev. D **73**, 067302 (2006)[astro-ph/0412535]
- [83] J. Skilling, <http://www.inference.phy.cam.ac.uk/bayesys/>
- [84] B. Feng, X. L. Wang and X. M. Zhang, Phys. Lett. B **607**, 35 (2005) [arXiv:astro-ph/0404224];  
M. Z. Li, B. Feng and X. M. Zhang, JCAP **0512**, 002 (2005) [arXiv:hep-th/0503268]